CHAPTER 2

NMO-Based Methods for Obtaining Images from Profiles

Sparse sampling of the data along the geophone axis and cable truncations introduce spurious semicircles into the output of the Cartesian method. These artifacts disappear when the downward continuation is done in an NMO-based coordinate system. Clean images are produced by the two NMO-related algorithms discussed in this chapter even when both the shot and the geophone axes are sparsely sampled. The first algorithm consists simply of the NMO and time-to-depth correction of profiles. The second is a pre-stack migration of profiles in radial/NMO coordinates.

The first section of this chapter discusses the NMO and time-to-depth correction algorithm and its application to the profiles of a marine seismic line. The two succeeding sections derive a 15-degree one-way wave equation for downward continuing upgoing waves in radial/NMO coordinates. This derivation is followed by a brief discussion of the form taken by imaging condition in radial/NMO coordinates. The first part of the final section is an exposition of the pre-processing and radial/NMO migration of a single profile. The final section of the chapter concludes with a description of the results of applying the method to a suite of profiles from a seismic line.

Normal moveout and time-to-depth correction

In regions where dips and lateral velocity variations are not too strong, migration is unnecessary. This motivates an easy way for obtaining images of the subsurface from profiles. The method involves stretching the traces according to NMO and time-to-depth correction formulae.

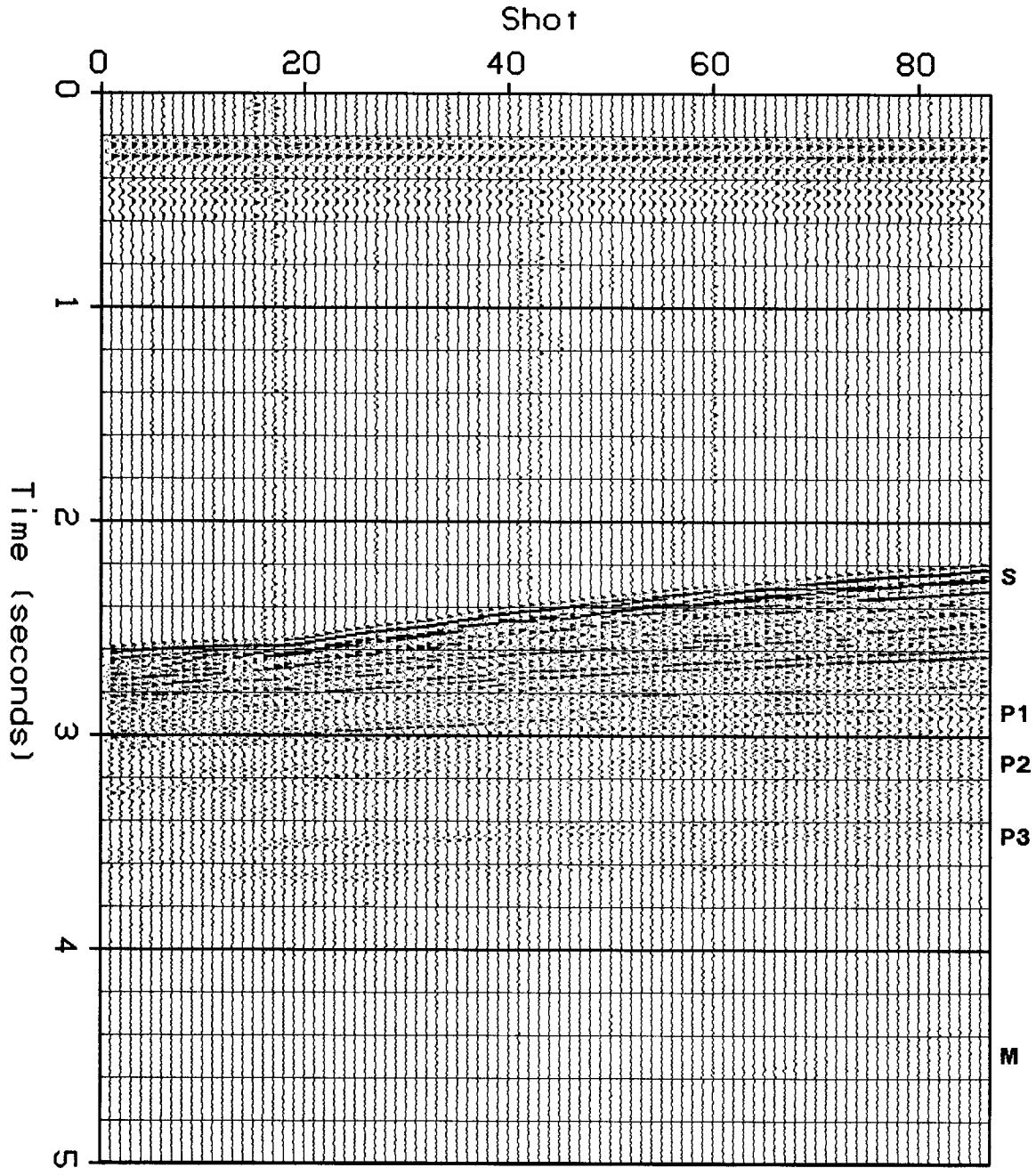

FIGURE 2.1. Near offset section. The near offsets from 86 consecutive profiles from a line recorded in the Gulf of Alaska by the USGS. The shots are 50 meters apart from one another. The direct wave is the event between 0.2 and 0.4 seconds. The sea floor is event **S** , stretching from 2.6 seconds on the left to 2.2 seconds on the right. Diffractions on the sea floor are visible near traces 20 and 65. Several primary reflections are at slightly larger travel times. Those marked **P1** , **P2** , and **P3** will be discussed later. Event **M** is a sea-floor multiple reflection.

Given an rms velocity function for a trace with offset h and midpoint y, the NMO correction formula maps one-way travel time t_0 into t. The correction

$$t^2 = 4t_0^2 + \frac{4h^2}{v_{rms}^2(y,t_0)}$$

is the same as that used to correct common midpoint gathers for the effects of offset. This formula makes sense as long as dips and lateral velocity variations are moderate.

If a depth section is desired, then the NMO coordinate t_0 must be converted to depth z. The process that accomplishes this change of coordinates is time-to-depth conversion. In the absence of dip, the depth of an event and its one-way vertical travel time are related by

$$t_0 = \int_0^z dz' \frac{1}{v(y,z')}$$

where v is the acoustic velocity function.

The NMO method of imaging was performed on 86 successive profiles from a marine seismic line from the Gulf of Alaska. The lateral velocity gradients were slight everywhere except at the sea floor. Therefore, the same velocity function was used to correct all the traces of a given profile. However, these rms velocity functions were allowed to vary from profile to profile. In total, 86 profiles, 48 traces per profile, 1250 samples per trace, were NMO corrected. The data was sampled at a 50 meter rate along the shot axis, a 50 meter rate along the geophone axis, and at a 4 millisecond rate along the time axis. The near offset distance was 238 meters on input, but the leading trace on output was some 643 meters to the far side of the shot from the hydrophones. The depth axis on output is sampled at a 10.57 meter rate. A near trace section and a plot of four seconds from the first seven shot profiles appear in figures 2.1 and 2.2, respectively.

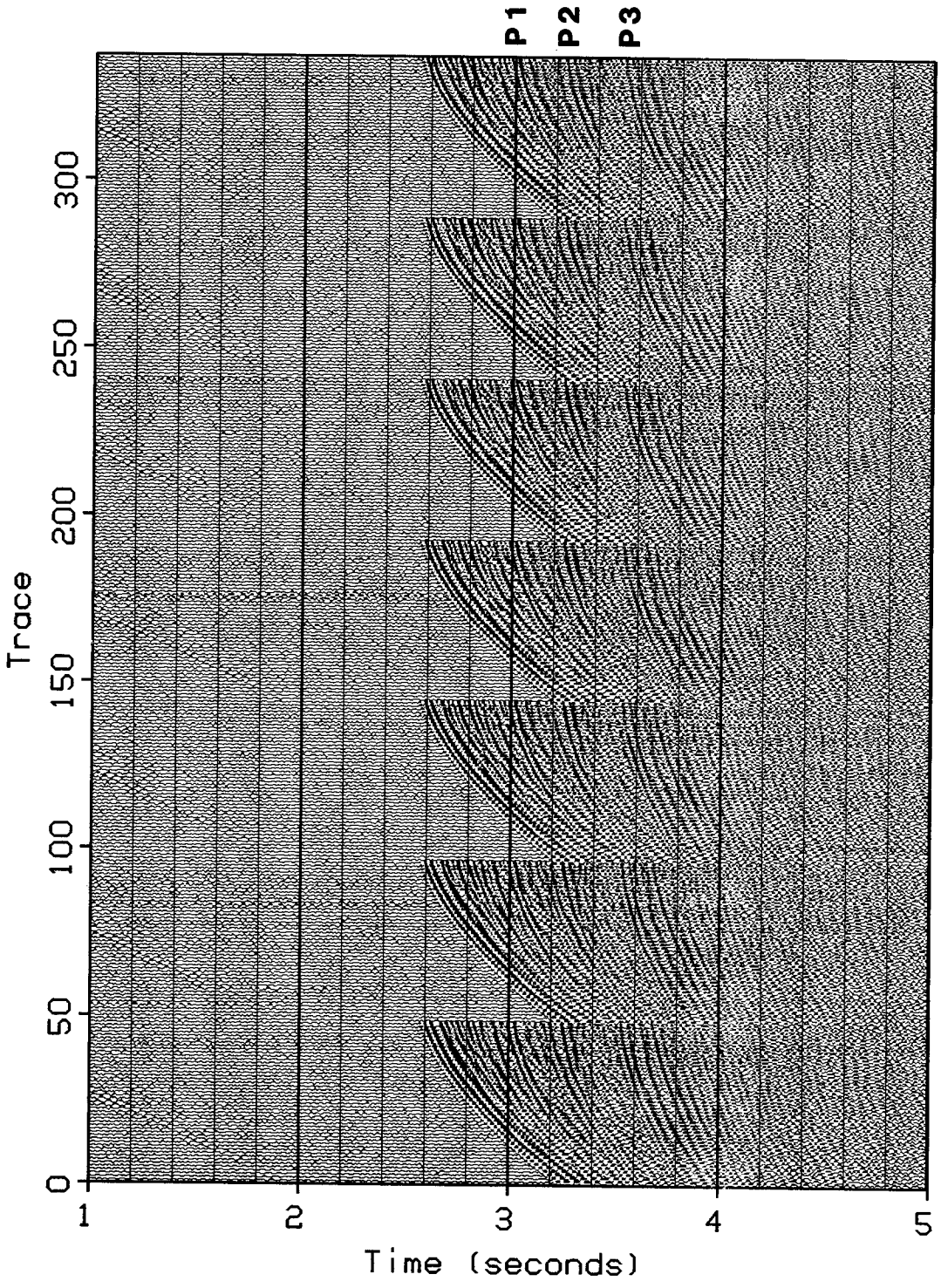

FIGURE 2.2. Profiles from the Gulf of Alaska line. The first seven profiles of the USGS Gulf of Alaska line. The first traces from each of these profiles are at the bottom of the page. The axis across the top of the page is time in seconds. The traces are plotted in order of occurrence from the bottom towards the top.

The near offset section should be carefully examined, because an understanding of its geometry will be useful in interpreting the shot profiles. It should be noted that no effort was made to remove either the bubble waveform or multiple reflections from the data. All attempts at bubble deconvolution decreased the lateral coherence drastically. On the other hand, multiples were left in the data to study their behavior under processes that form images from common shot profiles. Since the water is roughly 1.85 kilometers deep, the first few primary reflections and their sea-floor multiples are well separated from one another. If the events on the section are identified by their time of occurrence on trace number 86, the left-most trace, then a sea-floor primary can be identified at 2.2 seconds. The sea-floor reflection has several diffraction hyperbolas superimposed on it, reflecting a rough topography. The sea-floor reflection occurs at earlier times as the shot point index increases, corresponding to a sea-floor dip of about five degrees. Additional primary reflections occur at 2.6 and 3.4 seconds, with primaries having lateral amplitude variations, perhaps caused by the focusing and defocusing of the irregular sea-floor. These primaries also have an apparent dip that seems to be largely due the lateral variation in the size of the water column. Sea-floor multiples occur at 4.4 and 4.8 seconds on trace 86.

The water bottom reflection at 2.6 seconds and primary reflections at 3.0 and 3.5 seconds are easily identifiable on the shot profiles. The multiple is absent on the profiles of figure 2.1, because it is expected to occur at times later than 5.2 seconds in this part of the line. The multiple can, however, be observed to creep into the bottom of profiles later in the line when these are displayed sequentially. Such plots are easily made in movie form for display on a storage screen.

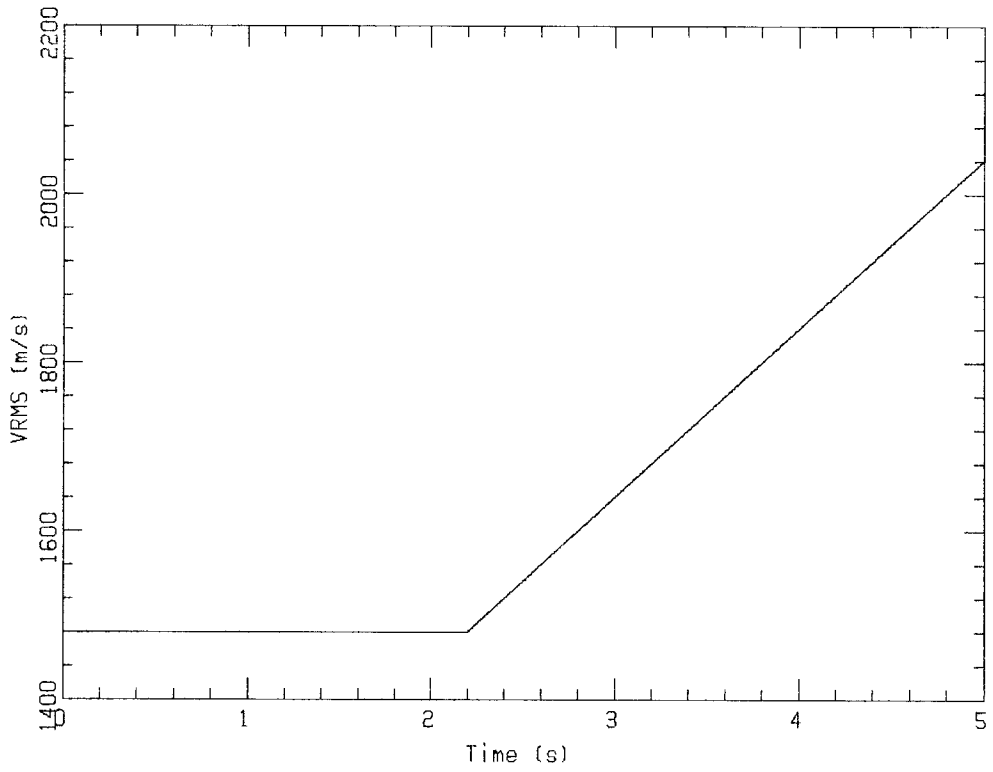

FIGURE 2.3. RMS velocity function for the Gulf of Alaska line. The *rms* velocity functions for the NMO correction of the data plotted in figure 2.2 were a function of shot position, but were kept independent of g within each profile. The functions are almost linearly dependent on travel time below the seafloor reflection intercept.

Fortunately, the seismic line was accompanied by the results of *rms* velocity measurements at several of its midpoints. From these measurements, *rms* velocity functions were estimated for use on common shot profiles. The function for the first shot profile of the line appears in figure 2.3. By performing normal moveout and time-to-depth conversion, an estimate of the positions of the reflectors beneath the shot profiles can be made. The result for the first seven profiles is plotted in figure 2.4. The output has been effectively subsampled by deleting every other trace to make it look more like figure 2.16, a plot of the same

shot profiles after wave equation migration (really figure 2.4 was generated by passing the data through every step of the migration procedure used to generate figure 2.16 except those steps involving data extrapolations at near and far offsets and the step involving an application of the 15-degree wave equation operator). The padding in figure 2.4 was put there for the same reason, to make the job of comparing migrated and unmigrated NMO corrected shot profiles easier.

The radial/NMO coordinate system for imaging profiles

Simple normal moveout and time-to-depth corrections do not correctly position events in space when there are dipping reflectors. A migration of the profiles is necessary to correctly position such interfaces. If insensitivity to the geophone sampling rate is desired, then a migration method that works in a coordinate system defined by the normal moveout correction is appropriate.

The data most likely to be aliased on a shot profile recorded in an area with minor deviations from layer cake geology is that lying at large offsets. Normal moveout alleviates the problem for primary reflections from planar interfaces with near-zero dip. For instance, a cursory comparison of figures 2.2 and 2.4, shows that the range of stepouts has been markedly reduced by applying a normal moveout correction. If a normal moveout coordinate system is used for migrating seismic data recorded over a favorable geology, then migration amounts to a time-to-depth conversion plus a small amount of lateral and vertical shifting. The job is so simple that a low order (15-degree) differential equation with a large step size can be used. Utilization of a 15-degree equation with a large step size makes for a pre-stack migration at minimal cost.

Further reductions in the effort involved in pre-stack migration are obtained with cylindrical, instead of the usual Cartesian, coordinate system. The angular coordinate of such a system is related to the ray parameter of a plane acoustic

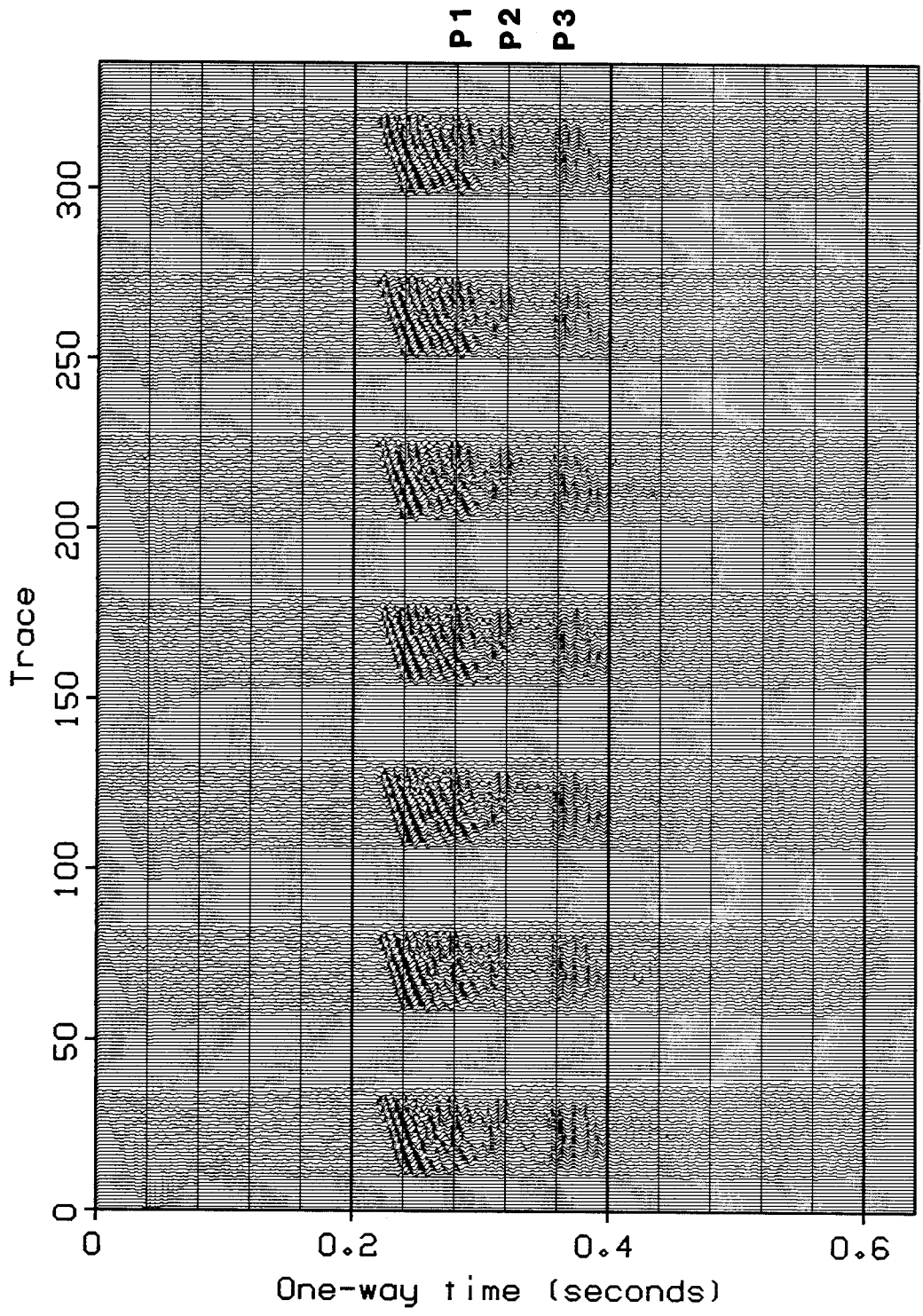

FIGURE 2.4. NMO corrected profiles. The first seven profiles of the USGS Gulf of Alaska line. The profiles have been NMO and time-to-depth corrected. The vertical axis is sampled at a rate of 17.5 meters, so the sea floor image occurs at a depth of about 1960 meters.

wave. The ray parameter of a ray propagating in a layer cake-like earth is an invariant function of the depth. Thus, if radial coordinates are used for migrating events caused by reflectors with near-zero dips, then a migration will involve some vertical shifts and still smaller "lateral" shifts of energy from one ray coordinate value to neighboring ray parameters.

The simultaneous use of a radial and NMO coordinates for the migration of data recorded over a regions with small dips should involve a minimum of effort. Moreover, the use of radial coordinates eases the boundary condition problem at the far offsets, since a boundary condition that forces the wavefield to equal zero at the ray parameter corresponding to horizontal propagation is a natural one. The other side boundary still presents a problem. In this study, a zero-slope boundary condition was enforced at the small-r side of the data while it was downward continued.

Radial/NMO coordinates are ideal for waves traveling along the rays sketched in figure 2.5. The new coordinate system requires the specification of a constant velocity parameter v_0. The transformation from the offset-time-depth coordinate system to radial/NMO coordinates is a set of three equations

$$\begin{aligned} r(g,t,z) &= \frac{g}{v_0^2\, t} \\ d(g,t,z) &= \frac{1}{2}\left[z + \left(v_0^2 t^2 - g^2\right)^{1/2}\right] \\ z'(g,t,z) &= z \end{aligned} \tag{1}$$

where v_0 is a constant acoustic velocity and the origin is at the shotpoint. The inverse transformation, form radial/NMO coordinates to recording coordinates, is easier to visualize. It is also more important, since the computer implementation of the algorithm for migrating NMO corrected profiles in radial/NMO coordinates uses the inverse transformation to map the data into radial/NMO space. Again, there are three equations:

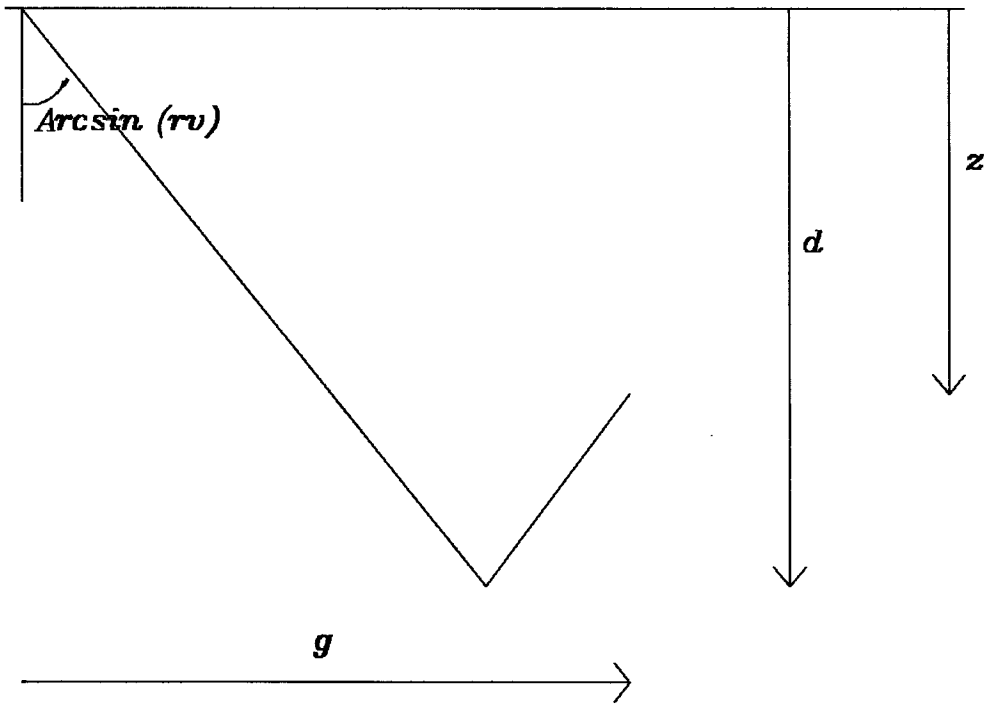

FIGURE 2.5. Radial/NMO coordinates. Recording coordinates are g, the distance from shot to phone, z, the depth of the downward continued phones z, and t, the travel time from shot to reflector to geophone. Radial/NMO coordinates are r, the sine of the angle of propagation, z, and d, the reflector depth.

$$
\begin{aligned}
g(r,d,z') &= \frac{(2d - z')\, r\, v_0}{\left(1 - r^2 v_0^2\right)^{1/2}} \\
t(r,d,z') &= \frac{2d - z'}{v_0\left(1 - r^2 v_0^2\right)^{1/2}} \\
z(r,d,z') &= z'
\end{aligned}
\tag{2}
$$

When $z' = z = 0$, implementation involves finding, for each pair (r_0,d_0) in the output space, the value of the input field at the corresponding pair (g_0,t_0), given by the inverse transformation of equation (2). In general (g_0,t_0) will not be a grid point of the input, so some interpolation will be necessary. All the examples of this section used a four point linear interpolation scheme to interpolate along a

line in (g,t)-space. The line chosen is the tangent to the zero-dip reflector travel time curve through the point (g_0,t_0). The slope of such a line is easily found to be equal to $g/(v_0^2 t)$. Not coincidentally, this slope is identical to r.

The radial/NMO 15-degree wave equation

A shot profile in any coordinate system can be treated as a boundary condition for a one-way wave equation. If that one-way wave equation is the 15-degree equation, then it can be written in radial/NMO coordinates by using the chain rule. From equations (2), the substitutions

$$\begin{aligned}
\frac{\partial}{\partial g} &= \frac{1}{v_0}\frac{\left(1 - r^2 v_0^2\right)^{1/2}}{(2\,d - z')}\frac{\partial}{\partial r} - \frac{1}{2}\frac{r v_0}{\left(1 - r^2 v_0^2\right)^{1/2}}\frac{\partial}{\partial d} \\
\frac{\partial}{\partial t} &= -\frac{r v_0\left(1 - r^2 v_0^2\right)^{1/2}}{2\,d - z'}\frac{\partial}{\partial r} + \frac{v_0}{2}\frac{1}{\left(1 - r^2 v_0^2\right)^{1/2}}\frac{\partial}{\partial d} \qquad (3) \\
\frac{\partial}{\partial z} &= \frac{1}{2}\frac{\partial}{\partial d} + \frac{\partial}{\partial z'}
\end{aligned}$$

must be made to express the one-way wave equation for upgoing waves in radial/NMO coordinates. For a constant acoustic velocity v_0 the one-way wave equation for an upwards propagating wavefield P in a single shot experiment takes the form

$$\frac{\partial P}{\partial z} = \left(\frac{1}{v_0^2}\frac{\partial^2}{\partial t^2} - \frac{\partial^2}{\partial g^2}\right)^{1/2} P \qquad (4)$$

The direction of propagation is controlled by the way the square root is defined, and in this work the square root of an operator is defined by its continued fraction. Thus, if A and B are commutative operators, B is positive-definite, and A is positive (negative) semi-definite, then $(A + B)^{1/2}$ is an operator that is positive (negative) semi-definite. When A is strictly imaginary, the square root is non-negative imaginary. Thus, the square root in equation (4) is causal in the t-

direction when the time derivative is a causal derivative, and is anti-causal when the time derivative employed is an anti-causal derivative.

Substituting equations (3) into equation (4) yields a partial differential equation for propagating upgoing waves in radial/NMO coordinates. If first derivatives of the wavefield are ignored, and the prime on z' is dropped, then differential equation (4) looks like

$$\left[\frac{\partial}{\partial z}+\frac{1}{2}\frac{\partial}{\partial d}\right]P = \left[\frac{1}{4}\frac{\partial^2}{\partial d^2}-\frac{\left(1-r^2v_0^2\right)^2}{v_0^2(2d-z)^2}\frac{\partial^2}{\partial r^2}\right]^{1/2}P$$

in the new coordinate system. Dropping the first derivatives of the wavefield leaves the phase behavior of the 15-degree approximant intact, but alters the amplitude behavior. Since we are much more interested in timing shifts for velocity analysis and for good stacks, dropping these first derivatives leaves the 15-degree equation unaltered for all practical purposes. The square root can, as usual, be expanded as a continued fraction. Ignoring commutation relations, the expansion can be defined with the differential equation and recurrence relations

$$\left[\frac{\partial}{\partial z}+\frac{1}{2}\frac{\partial}{\partial d}\right]P = A_n P$$

$$A_0 = \frac{1}{2}\frac{\partial}{\partial d}$$

$$A_{k+1} = \frac{1}{2}\frac{\partial}{\partial d}-\frac{\dfrac{(1-r^2v_0^2)^2}{v_0^2(2d-z)^2}\dfrac{\partial^2}{\partial r^2}}{\dfrac{1}{2}\dfrac{\partial}{\partial d}+A_k}$$

where the use of A_1 leads to a 15-degree equation. If A_1 is used and denominators are cleared, the result is the differential equation

$$\frac{\partial^2}{\partial d\,\partial z}P = -\frac{\left(1-r^2v_0^2\right)^2}{v_0^2(2d-z)^2}\frac{\partial^2}{\partial r^2}P$$

that looks like the 15-degree equation geophysicists have become used to. The differences are that the coordinate system has been changed and the coefficient

in front of the second derivative with respect to the lateral "spatial" coordinate is no longer a constant.

The direction of propagation of equation (4) is defined, but its causality is not. The equation can be used to push an upgoing wavefield either downwards or upwards. Migration pushes the upgoing wavefield downwards, and does this by specifying the causality of the z and d derivatives that it uses. A causal z

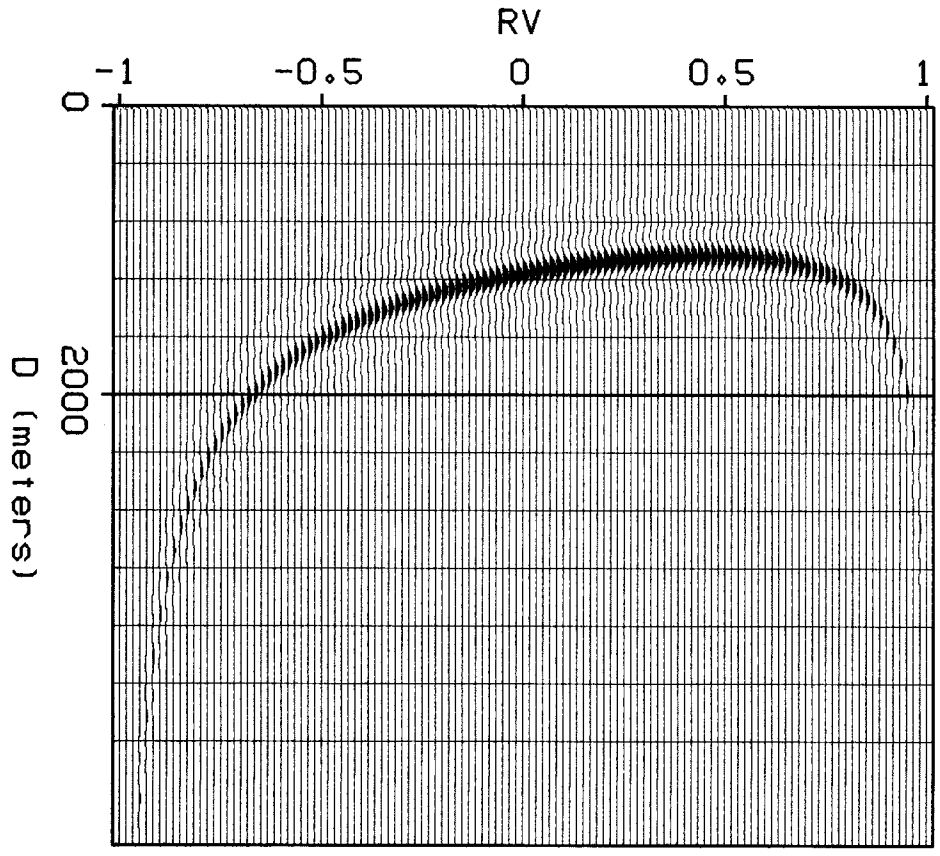

FIGURE 2.6. Point scatterer impulse response. The seismogram caused by a point scatterer transforms to this irregular shape in the (r,d) plane. The scatterer is located 1010 m below the surface and 500 m to the geophone side of the shot. The r axis is sampled at .011 ms/m and r = 0 is a vertical line through the center of the plot.

derivative and an anti-causal d derivative are employed, denoted by D_z and $(-D_d)^H$, respectively. Migration also makes use of both causal and anti-causal lateral derivatives, D_r and $(-D_r)^H$, respectively. With these choices, the 15-degree wave equation for migrating upgoing waves is

$$(-D_d)^H D_z \; P \;=\; \left[\frac{1 - r^2 v_0^2}{v_0(2d - z)} \right]^2 \; (-D_r)^H D_r \; P \qquad (5)$$

Since the right hand side of equation (5) has functions that are d-dependent, a Fourier transform over d does not lead to a simple frequency domain formulation of the wave equation. Hence, equation (5) was discretized and implemented in the d (time-like)-domain. The discrete version of equation (5) is applied recursively in the anti-causal d and the causal z directions, much as the old 15- or 45-degree time domain operators in (x,z,t)-space worked in the anti-causal t and causal z directions (the migration operator for upcoming waves pushes the field from $z = 0$ to positions where $z > 0$ and, at each z-step, from retarded travel time $t > 0$ to $t = 0$).

The imaging condition in radial/NMO coordinates

An image can be obtained from a downward continued shot profile by cross-correlating the downgoing wave caused by the shot with the upgoing wave recorded at the geophones. The image then appears at the zero-time lag of this cross-correlation. This imaging condition takes a peculiarly simple form in the radial/NMO coordinate system.

The downgoing wave, or direct wave, on a shot profile can be modeled as an amplitude modulated delta function. In (g,z,t)-space, this delta function takes the form

$$D(g,z,t) \;=\; \frac{\delta(t - \left[g^2 + z^2\right]^{1/2} / v_0)}{t^{1/2}}$$

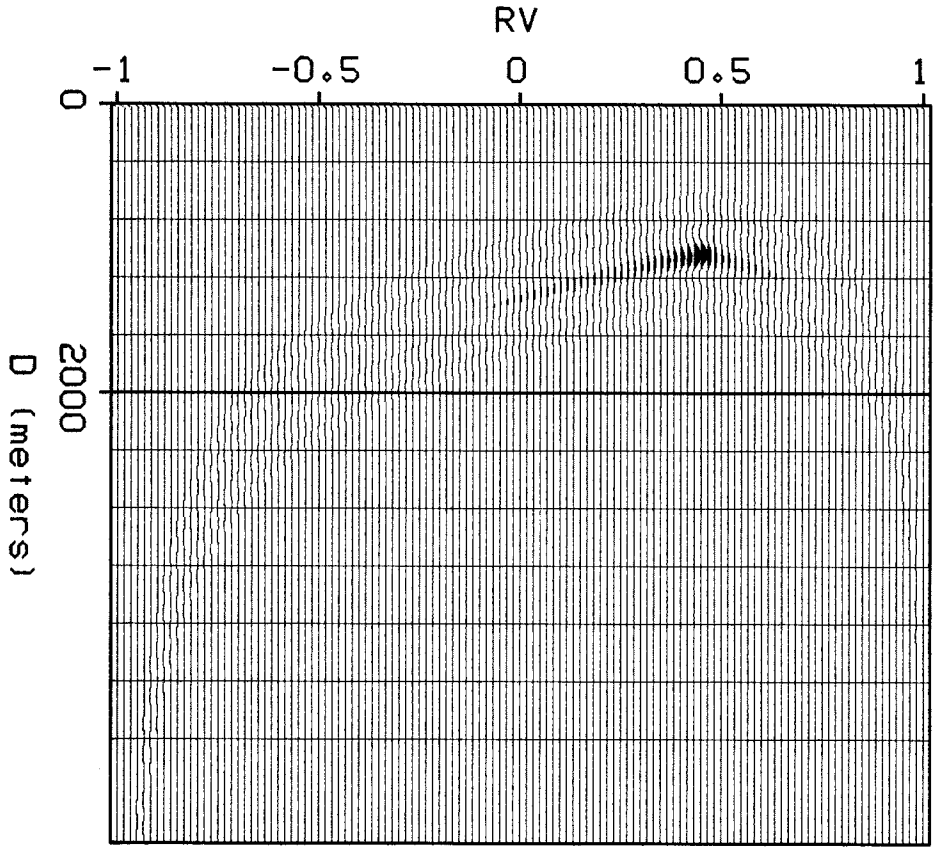

FIGURE 2.7. Downward continuation of a point response. When the geophones are 1000 m below the surface, the point scatterer seismogram has a sharp peak at the image point with two tails attached to it.

The delta function is equal to zero at all points where its argument is non-zero. Since D is to be cross-correlated with another wave, the set where it is non-zero is of particular interest. Using equations (2), the values where the delta function is non-zero are given by

$$\frac{2d-z}{\left(1-r^2v_0^2\right)^{1/2}} = \left[\frac{(2d-z)^2r^2v_0^2}{1-r^2v_0^2} + z^2\right]^{1/2}$$

where a positive square root is understood. Squaring both sides of this equation

and eliminating r leads to a timing condition for image formation: $z = d$. Combining the condition $z = d$, equation (2) for $t(r,d,z')$, and the expression for $D(g,z,t)$, yields a functional form for the downgoing, direct wave in (r,z,d)-space

$$D(r,z,d) = \frac{\left[v_0^2(1 - r^2 v_0^2)\right]^{1/4}}{z}\delta(d - z) \tag{6}$$

If amplitude effects are ignored, then the imaging condition for downward continued common shot profiles in (r,z,d)-space is $d = z$.

An image in (r,z')-space is useless because geology occurs in the (g,z)-plane. The transformation to (g,z)-space can be had by plugging the imaging condition $d = z'$ into equations (2). Doing this and solving for r and z' yields the transformation equations

$$r = \frac{g}{v_0\left[z^2 + g^2\right]} \tag{7}$$

$$z' = z$$

for images made from common shot profiles. The image that is destined to appear at output coordinates (g,z) can be obtained from the image point given by equations (7) in radial/NMO coordinates.

The range g is allowed to sweep over is still arbitrary. An option that works well is to let h range over a segment about as long as the input data. The near offset distance should be at most equal to half the near offset distance before migration, less some length for padding. The output should probably include some traces with negative offsets.

Point scatterers in radial/NMO coordinates

In the previous section, an analytic expression for the downgoing, direct wave caused by the shot was derived. Analytic expressions for the upgoing

wave caused by a point scatterer at depth will be presented in this section.

Once again, the recorded wave can be modeled as an amplitude modulated delta function. This delta function is non-zero when t is equal to the sum of the travel time from the shot to the scatterer with the travel time from the scatterer to the geophone. Placing the shot at the origin, the scatterer at position (g_0,z_0), and geophones at positions (g,z), the upgoing wave takes the form

$$U(g,z,t) = \frac{v_0^{1/2}}{\left[(g-g_0)^2 + (z-z_0)^2\right]^{1/4}} \delta\left(t - t_0 - \frac{1}{v_0}\left[(g-g_0)^2 + (z-z_0)^2\right]^{1/2}\right)$$

where t_0 is the travel time from the shot to the scatterer. Since t_0 is independent of g, z, and t, it is a true constant. The amplitude of U is also a function of shot position, but this dependence has been neglected to simplify the analysis.

The wave $U(g,z,t)$ is equal to zero at most points in (g,z,t)-space. The only places where U does not vanish are those where the argument to the delta function is equal to zero. In (r,z,d)-space, this happens when the following equality holds:

$$\frac{(2d-z)}{v_0\left(1 - r^2v_0^2\right)^{1/2}} + t_0 = \frac{1}{v_0}\left\{\left[\frac{(2d-z)rv_0}{\left(1 - r^2v_0^2\right)^{1/2}} - g_0\right]^2 + (z-z_0)^2\right\}^{1/2}$$

When $d \geq z$ and $|rv_0| < 1$, both sides of the equality are non-negative, so the expression is well defined. Squaring both sides of this equation and then manipulating the result to isolate the term $(2d-z)$, yields a quadratic equation

$$(2d-z)^2 - \frac{2(vt_0 - rv_0g_0)}{\left(1 - r^2v_0^2\right)^{1/2}}(2d-z) + \left[v_0^2t_0^2 - (z-z_0)^2 - g_0^2\right] = 0$$

with two real roots. One of these two roots seems not to have any physical significance. Keeping only the root that has a physical meaning and solving for d, yields an equation for the points in (r,z,d)-space where U is non-zero

$$d = \frac{z}{2} + \frac{v_0 t_0 - r v_0 g_0}{2\left(1 - r^2 v_0^2\right)^{1/2}} + \frac{1}{2}\left\{\frac{(v_0 t_0 - r v_0 g_0)^2}{1 - r^2 v_0^2} + \left[g_0^2 + (z - z_0)^2 - v_0^2 t_0^2\right]\right\}^{1/2}$$

The amplitude distribution of U in NMO/radial coordinates can be obtained by simple change of variables. The upgoing wave caused by a point scatterer in (r,z,d)-space is found to be equal to

$$U(r,z,d) = \frac{v_0^{1/2}}{\left\{\left[\frac{(2d - z) r v_0}{\left(1 - r^2 v_0^2\right)^{1/2}} - g_0\right]^2 + (z - z_0)^2\right\}^{1/4}} \qquad (8)$$

$$\delta\left[d - \frac{z}{2} - \frac{v_0 t_0 - r v_0 g_0}{2\left(1 - r^2 v_0^2\right)^{1/2}} - \frac{1}{2}\left\{\frac{(v_0 t_0 - r v_0 g_0)^2}{1 - r^2 v_0^2} + \left[g_0^2 + (z - z_0)^2 - v_0^2 t_0^2\right]\right\}^{1/2}\right.$$

Among the special cases of equation (8) that can be examined, the most interesting is that obtained by setting z, the depth of the downward continued geophones, equal to z_0, the depth of the scatterer. When this is done, the amplitude of $U(r,z,d)$ is singular at $r v_0 t_0 = g_0$. In (g,z,t)- space, this singularity condition is equivalent to $g = g_0$. The field obeys one of two equations defined on the two sides of the singularity. For $r v_0^2 t_0 < g_0$

$$U(r,z_0,d) = \left[\frac{v_0}{\left|\frac{(2d - z_0) r v_0}{\left(1 - r^2 v_0^2\right)^{1/2}} - g_0\right|}\right]^{1/2} \delta\left[d - \frac{z_0}{2} - \frac{(1 - r v_0)(g_0 + v_0 t_0)}{2\left(1 - r^2 v_0^2\right)^{1/2}}\right]$$

the wave travels towards negative r. In (g,z,t) space, this is a wave traveling horizontally towards negative g in the region $g < g_0$. Similarly, for $r v_0^2 t_0 > g_0$,

$$U(r,z_0,d) = \left[\frac{v_0}{\left|\frac{(2d - z_0) r v_0}{\left(1 - r^2 v_0^2\right)^{1/2}} - g_0\right|}\right]^{1/2} \delta\left[d - \frac{z_0}{2} - \frac{(1 + r v_0)(-g_0 + v_0 t_0)}{2\left(1 - r^2 v_0^2\right)^{1/2}}\right]$$

representing a wave traveling towards positive g in the region $g > g_0$.

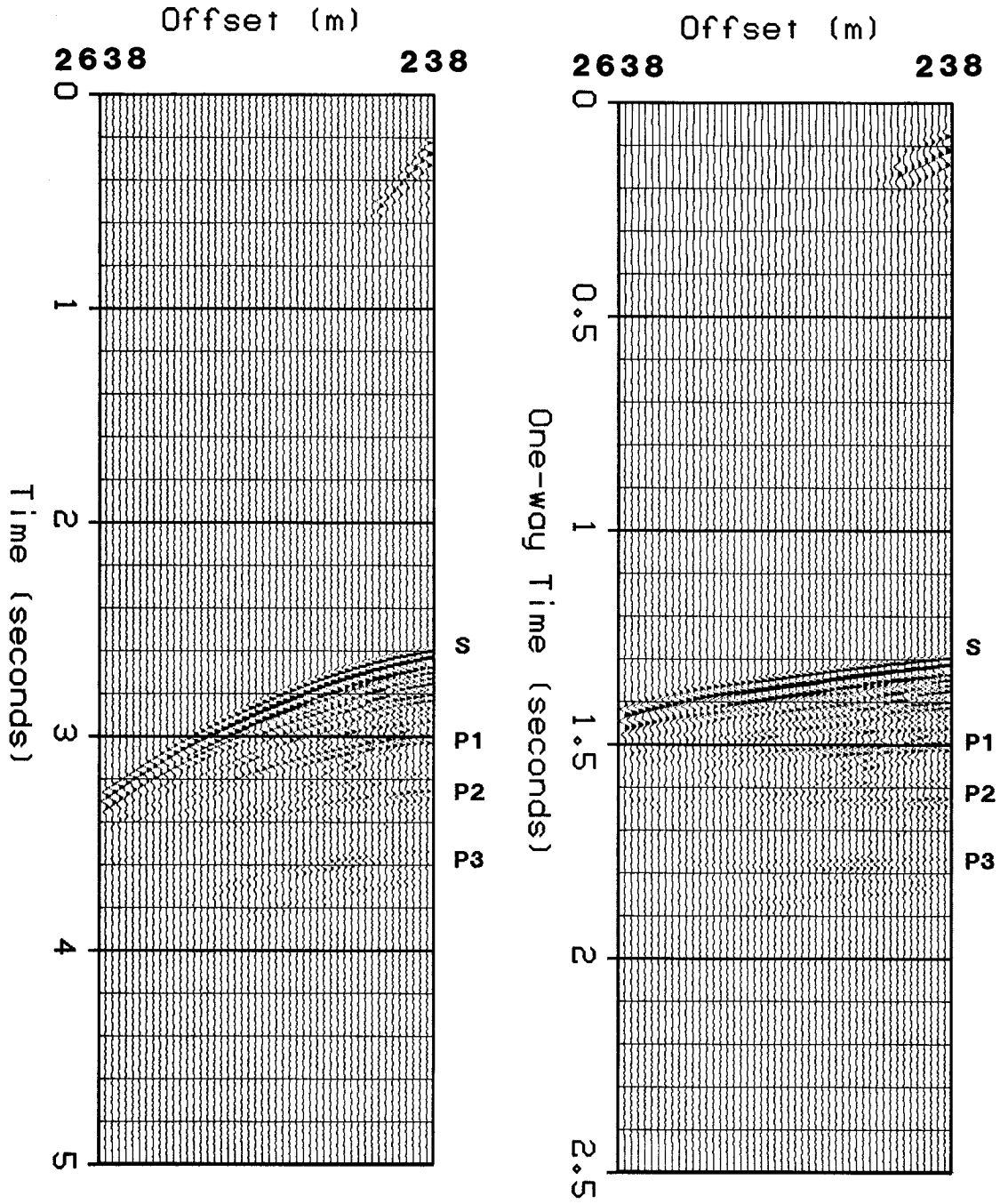

Left: **FIGURE 2.8. Input profile.** Raw data for the radial/NMO method of profile migration. The near offset, 238 meters distant from the shot is at the right edge. Right: **FIGURE 2.9. NMO correction.** The input has been NMO corrected with the *rms* velocity of figure 2.3. Since the sea floor reflector has a dip of about six degrees, the event at 1.3 seconds has not been flattened.

The transformation and migration of profiles

The pre- and post-processing for profile migration is complex, involving many steps. Plots of some steps are invaluable in judging the propriety of the many approximations used by a radial/NMO migration algorithm.

The new coordinate system is defined with a constant transformation velocity, so the first problem that arises is that of coping with vertically varying acoustic velocity. One solution is to convert the input data so that it looks like a profile recorded over a constant velocity earth. This can be achieved by applying an NMO correction with a time varying rms velocity function, converting from time to depth, and then applying an inverse NMO correction with a constant transformation velocity v_0. Figures 2.8 through 2.11 illustrate this step, as applied to the left-most profile of figure 2.2.

After conversion into a constant velocity profile, some pre-processing is still needed to lessen the effect of near and far offset data truncations. The data is therefore padded and the padding filled with an extension of the original data. In figure 2.12 the 48 traces of the input have been padded with six traces of zeros on the left and six traces of zeros on the right. The bottom was padded with a mere four samples. The padding was filled in by (1) applying a spherical divergence conversion to make the data more stationary, (2) applying a normal moveout correction to reduce the range of stepouts and change most events so that they are linear and horizontal, (3) transposing the NMO corrected data, (4) convolving the transpose with a time-domain recursive dip filter set to reject high dips, (5) transposing the filtrate, (6) restoring the normal moveout, (7) restoring spherical divergence, and (8) restoring the input data.

After extrapolation, the profile was gained to make to appear as if it were recorded in a two dimensional world, and mapped into the radial/NMO coordinate

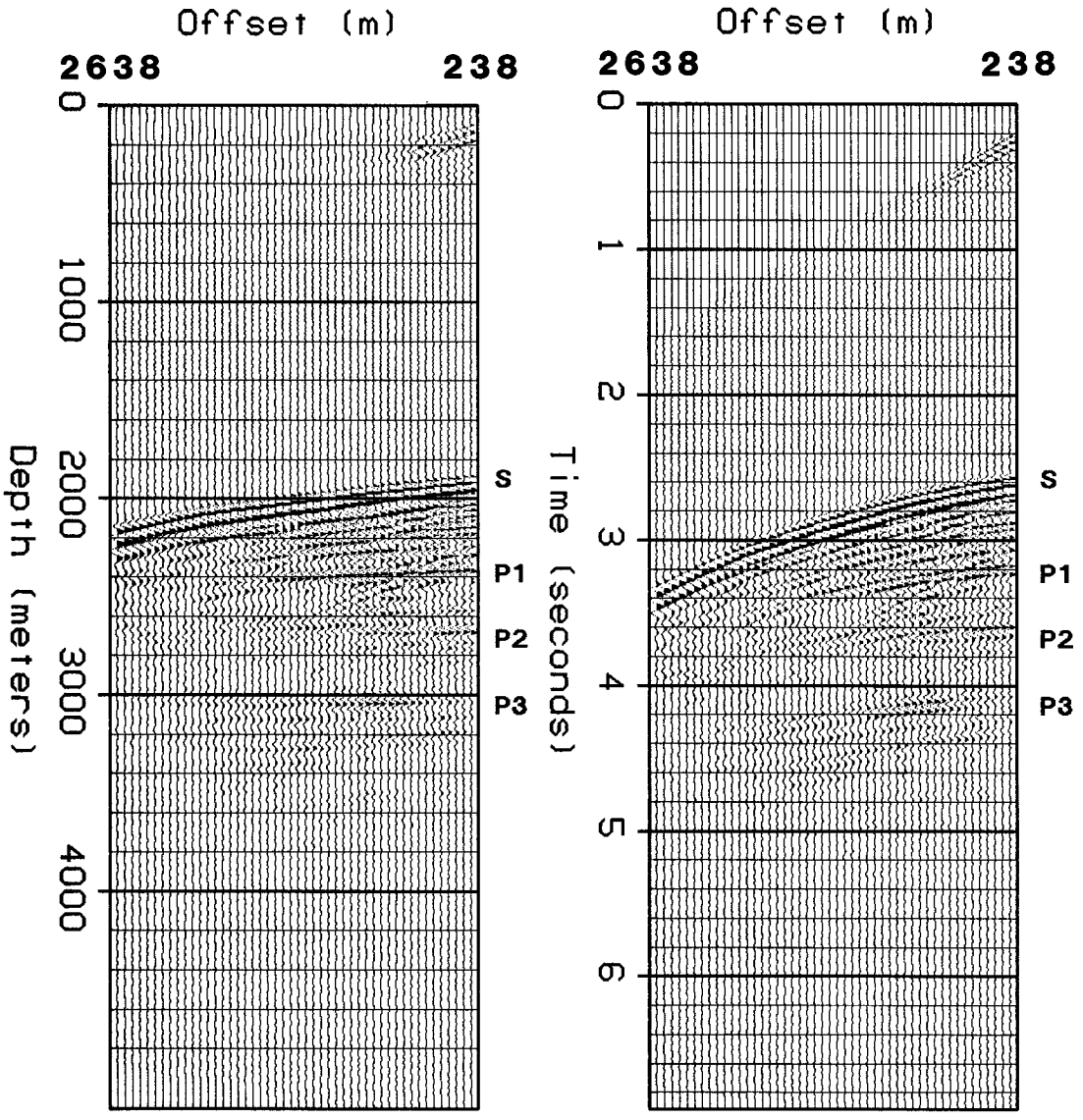

Left: **FIGURE 2.10. Time-to-depth correction.** The result of applying a time-to-depth conversion routine to figure 2.9. Right: **FIGURE 2.11. Inverse NMO correction.** The result of applying a constant velocity inverse NMO correction with a transformation velocity of 1480 m/s.

system. The transformation velocity was set equal to the minimum of the interval velocity function. The interval velocity function was constructed from the rms velocity used for normal moveout correction. If a larger transformation velocity is used, then there is a chance that some event will map into regions where rv_0

exceeds unity. Since waves with ray parameters this large do not propagate, the choice of v_0 as the smallest interval velocity is the cheapest transformation velocity that does not artificially create evanescent energy.

To build a mapping into the radial/NMO coordinate system, not only does a transformation velocity need to be specified, but some discretization parameters need to be chosen as well. The r axis was discretized with as many sample points between $r = 0$ and $r = 1/v_0$ inclusive as points in the padded input. Similarly, the d-axis was discretized so that there were as many sample points between $d = 0$ and the maximum depth expected inclusive as time samples in the input, scaled by the quotient of the maximum frequency in the signal by the Nyquist frequency.

The data as a function of r and d is plotted in figure 2.13. The result consists of a series of roughly horizontal bands. In general, the derivative with respect to r within such a band will be small. Thus, the effect of undersampling the geophone axis has been effectively minimized by the transformation into NMO coordinates. This was expected, because the dips present on the near offset section were all less than ten degrees. The shortness of the bands is a bit more troublesome. The data at high d has almost certainly been undersampled. The only correction for this is to sample the r-axis at a higher rate and bear the increased cost of migration. The higher r values seem not to be present in the data, so one option that would decrease costs is to insist that the wave contain no events between some preset value r_0 and 1. Unfortunately, it is hard to tell if a profile other than that displayed might not contain an event with a large ray parameter or if any of the profiles of the line might not, after migration, contain such an event.

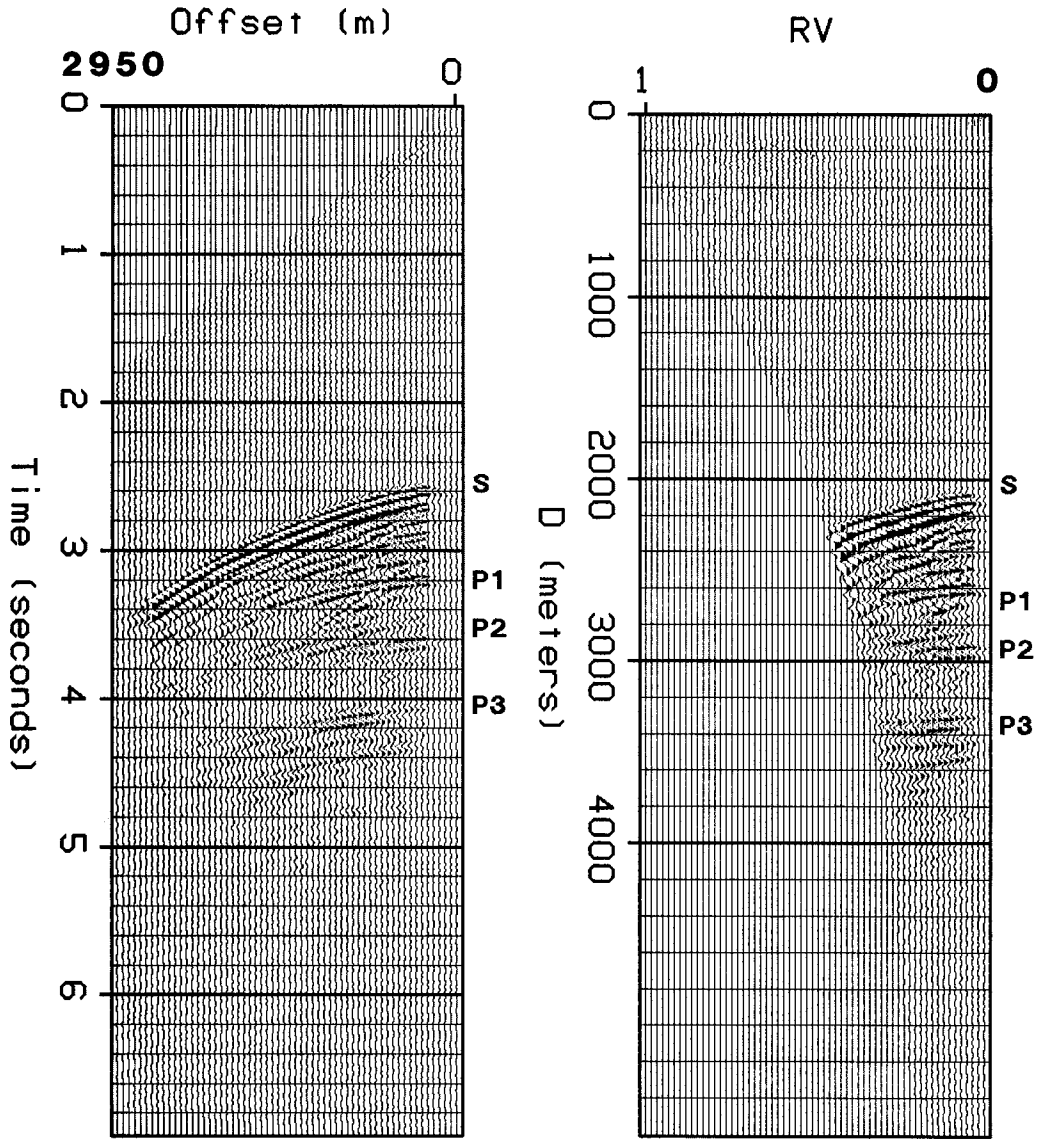

Left: **FIGURE 2.12. Padding and extrapolation.** The data has been padded and extrapolated to suppress the truncation effects at far and near offsets. The extrapolation process consists of NMO correction, low-pass dip filtering, and restoration of the recorded data between the padding at the sides. Extrapolation is done to suppress smiles created while downward continuing. Right: **FIGURE 2.13. Radial/NMO coordinate mapping.** After padding, the data is mapped from (g,t)-coordinates into the coordinate system with r and d-axes. The data is sampled along the r axis at a rate of 11.26 milliseconds per kilometer. The sampling interval for d is 10.57 meters. The sampling in the r direction is too coarse, since the grid is vacant at regions where rv is near unity.

Finally, the profile was migrated and imaged. Plots of the image plane in (τ,d,z)-space and the image in (g,z)-space appear in figures 2.14 and 2.15. Since Δz was chosen to be equal to 10 times Δd, the image plane's gradient was equal to 10 and lay in the plane $\tau = 0$. Only the volume beneath the image plane is involved in the migration process because of the causality of the derivatives used in migration. The computational cost associated with downward continuing geophones is proportional to the volume of the active set beneath the image plane. It follows that choices of Δz smaller than the one used, even though they would have generated a cleaner image, involve much higher cost. The price paid for speed is the clutter at the image of the sea floor. As little oil can be expected to be trapped at the sea floor and since the images of the other events seem clean, perhaps the large z step size is justified.

As promised, the profiles of the USGS Gulf of Alaska line were migrated. Migrating a whole line of profiles is much more interesting than migrating an isolated profile because lateral velocity anomalies should be visible. If the data from the migrated profiles are reorganized into data sets sharing a common receiver, a so-called geophone profile, then pictures of the subsurface obtained with different illumination angles are obtained. If the shot profile images are made with a correct velocity estimate, then the depth estimates of the various reflectors will be independent of illumination. On the other hand, if the shot profile images are made with a slightly incorrect velocity estimate, then the depth estimates will be slightly illumination dependent. For instance, if the velocity is a little too high, then the depth estimates will be larger for big offsets than for small offsets. If these travel time anomalies can be estimated reliably, then they can be converted into migration velocity field perturbations.

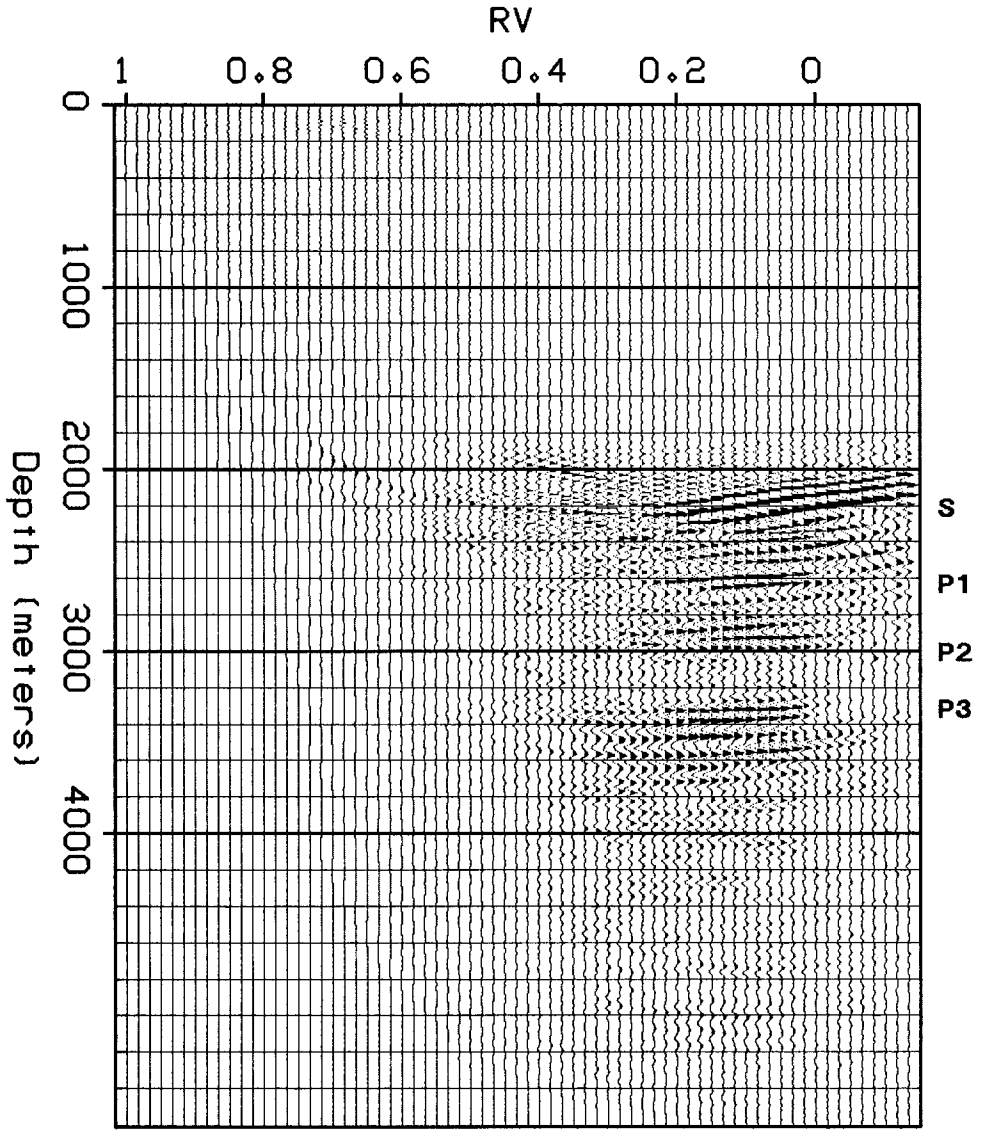

FIGURE 2.14. A migrated image plane in radial coordinates. After migration the image plane is in the coordinate system with r and z-axes. The sampling interval along the z-axis is 10.57 meters. The sampling along the r-axis is the same as that in figure 2.13, 11.26 milliseconds per kilometer. The data has been padded on the right to make room for data moving into regions of the plane where r is small. The origin of the coordinate system is marked in the plot.

The Gulf of Alaska line was migrated with time shifted versions of the velocity function plotted in figure 2.3. The time shift was obtained by picking the zero offset travel time of the sea floor reflection on each of the gathers of the line. The first seven profiles are again plotted, this time in figure 2.16. The migrated output and the NMO corrected input to the migration program (see figure 2.4) are different. Most of the events on the image in figure 2.16 have shifted upwards and towards zero offset. The only exception is an event at a depth of about 3000 meters that has near-zero dip. The padding in the migrated output is filled with migration smiles that should be considered as processing artifacts. All events wobble as a function of shot position. This wobble is probably caused by lateral velocity perturbation, so in principle a measurement of the wobble can be translated into an estimate of the perturbation.

A comparison of the two shot profile migration procedures

The Cartesian and NMO-coordinate methods have been applied to the same shot profile, but the two images are different. The main reason for the difference is that the migration velocity used by the Cartesian method accounted for the dip in the sea floor while the velocity used by the NMO-coordinate method was laterally invariant. Since the velocity used by the Cartesian method was closer to that of the earth, the events on the Cartesian method's image are more accurately positioned than corresponding events on the NMO-coordinate image.

Event	NMO Offset	NMO Depth	Cartesian Offset	Cartesian Depth
Sea floor	100	2100	150	2000
P1	350	2600	250	2450
P2	250	2925	250	2800
P3	400	3350	300	3200

TABLE 2.1. Primary events on the migration images. Events identified in the migration outputs plotted in figure 2.17. All units are in meters.

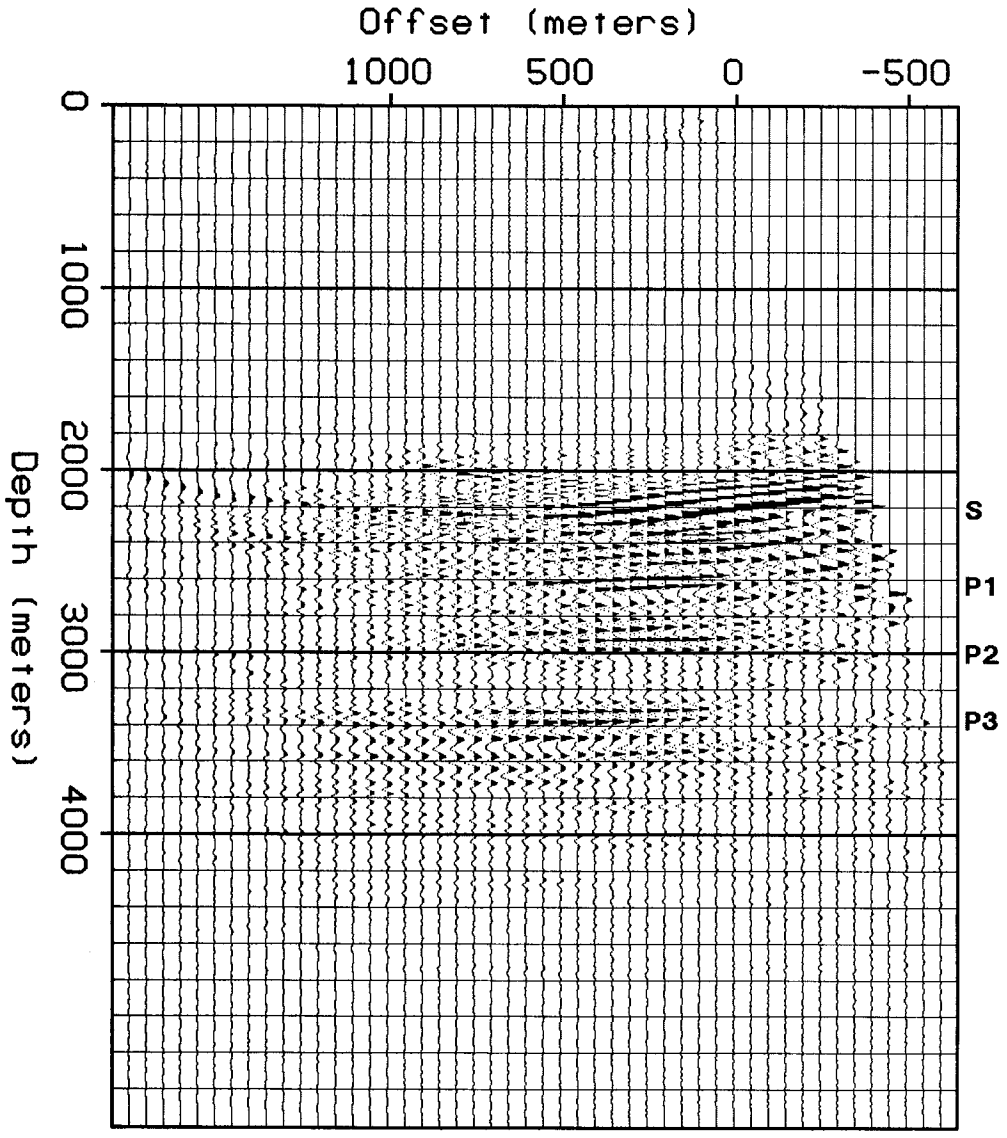

FIGURE 2.15. The image plane in the output coordinate system. The result of applying an $\tau \rightarrow g$ mapping to the data set in figure 2.14. The discretization and plotting parameters are the same as those used in figures 1.2 and 1.3. The data is sampled along the geophone axis every 50 meters. Here, the shot point lies 643.5 meters to the left of the rightmost trace.

An important difference between the two pictures is that events on the Cartesian image (figure 1.3) are consistently shallower than corresponding events on the NMO-coordinate image (figure 2.15). To make this difference easier to see, the two sets of data are windowed, non-linearly gained, and plotted adjacent to one another in figure 2.17. The non-linear gain applied tends to suppress small events. Four corresponding events in each half of figure 2.17 will be considered. Approximate offsets and depths for the four events on the two outputs are listed in table 2.1. The discrepancies in the table are the result of a low-velocity wedge, just above the sea floor, at a depth of 2000 meters. The Cartesian method honored this velocity anomaly, but the NMO-coordinate method ignored it. The main effect of the wedge is a vertical shift of events on the Cartesian image about those in the NMO-coordinate image. Table 2.1 also reveals a small lateral shift from the positions of corresponding events in the NMO-coordinate image.

An estimate of the size of the depth discrepancy caused by the low velocity wedge is easily obtained. The thicknesses of the wedge at near and far offsets are 25 and 277 meters, respectively. With a replacement velocity of 2000 meters per second, the wedge introduces a time delay that can be approximated by

$$\Delta t = (25\ m + 277\ m/\cos 30^\circ)\left(\frac{1}{1480\ m/s} - \frac{1}{2000\ m/s}\right) = 0.058\ s$$

if a vertical ray path at the near offset and a 30 degree ray path at the far offset are assumed. Ray tracing suggests that these numbers are reasonable. The time discrepancy occurs in a region with a velocity of about 2000 meters per second, so a 58 millisecond delay corresponds to a depth error of about 120 meters. Since the Cartesian method uses a slower velocity than the NMO-coordinate method, events on the Cartesian output will occur about 120 meters

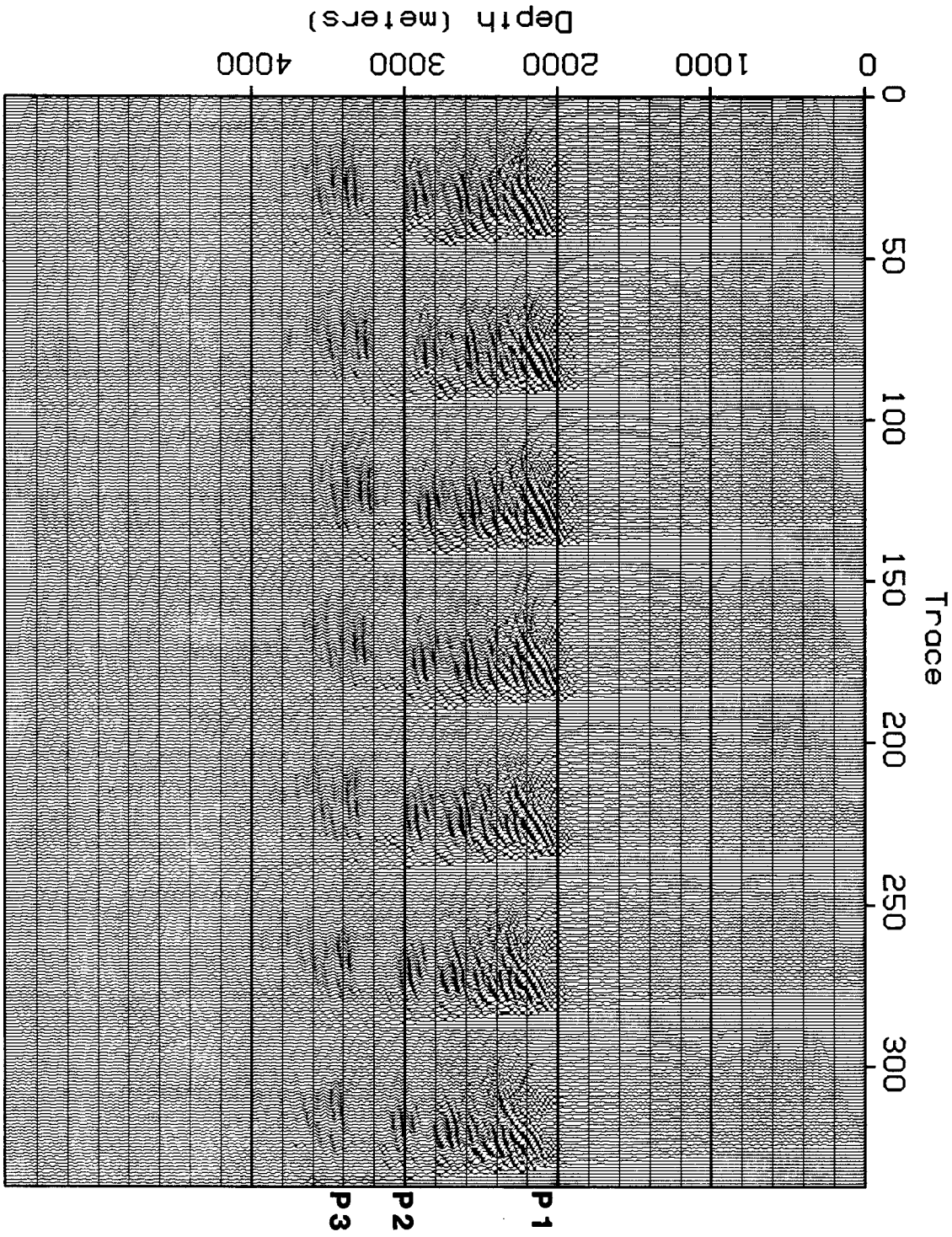

FIGURE 2.16. Profiles migrated with the radial/NMO method. The first seven profiles of the USGS Gulf of Alaska line. The profile have been migrated in radial/NMO coordinates. The data for figure 2.15 appears as traces indexed 0 through 47.

above corresponding events on the NMO-coordinate image. A quick glance at table 2.1 shows that this is indeed the case.

There are also some differences in the lateral placement of events on the two images. The lateral displacements are more difficult to measure than the vertical discrepancies because their determination relies on the identification locations with anomalous reflection coefficient. Though the scatter is large, the Cartesian migration tends to move events about 100 meters closer to zero offset than the NMO-coordinate method does. This effect, too, is a result of the laterally varying velocity model used by the Cartesian method.

Finally, an important difference between Cartesian and NMO-coordinate images is the sensitivity of the former to sampling along the geophone axis. Because the Cartesian algorithm requires derivatives with respect to g, its performance degrades when high lateral wavenumbers are present in its input. For instance, the sea floor reflector at 2000 meters depth is split into a sequence of laterally displaced images in figure 1.3. In comparison, the NMO-coordinate migration produced an image of the sea floor that has a better defined location and dip.

Radial/NMO coordinates for a vertically varying medium

The time-to-depth correction that made figure 2.14 possible is a coarse approximation. Over dipping beds, this correction is not well-defined and lead to misplacement of events in imaged common shot profiles. It would be preferable to develop and use a new coordinate system. Such a system is

$$g = 2\int_0^D \frac{rv(s)ds}{\left[1 - r^2v^2(s)\right]^{1/2}} - \int_0^{z'} \frac{rv(s)ds}{\left[1 - r^2v^2(s)\right]^{1/2}}$$

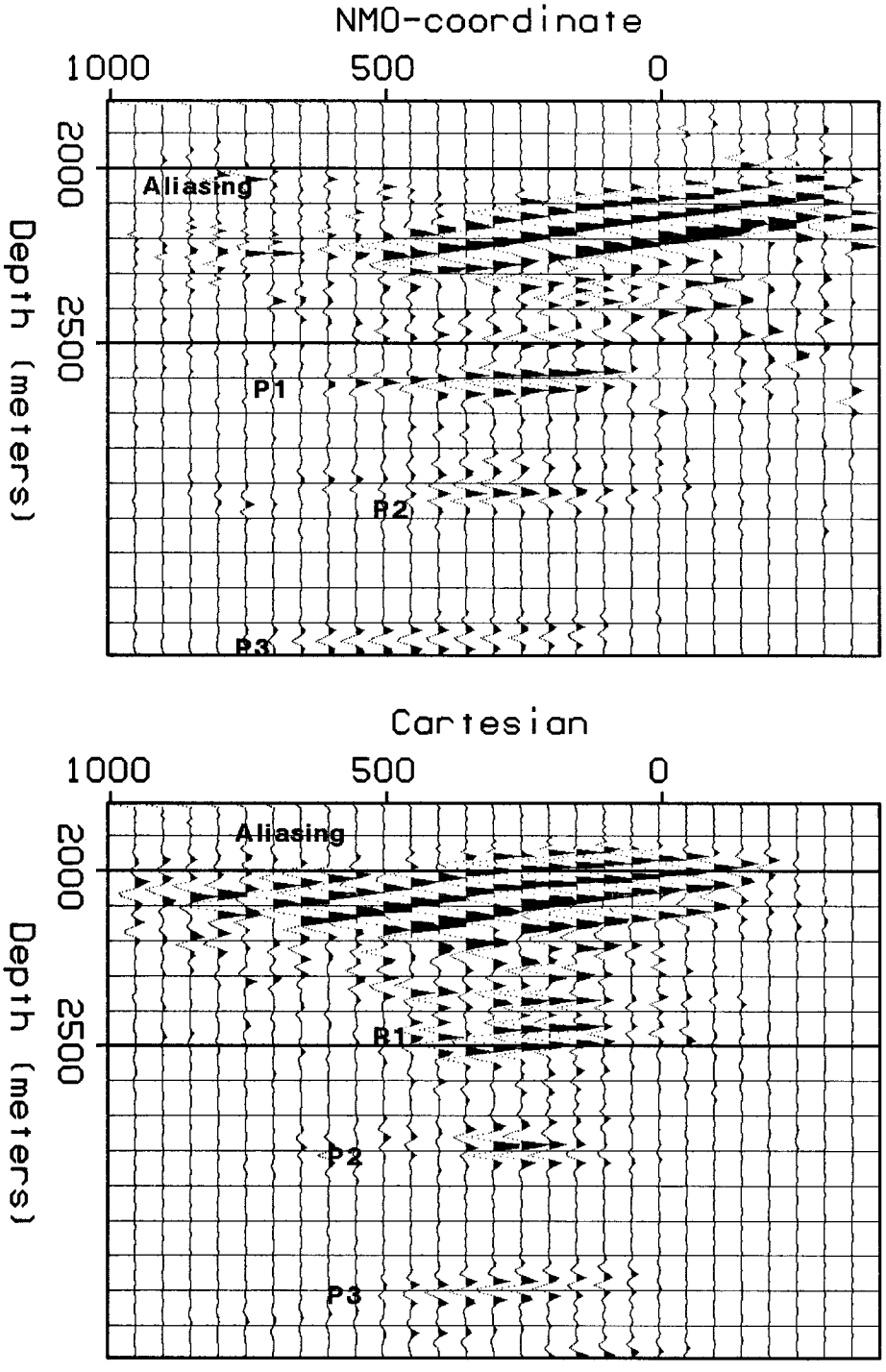

FIGURE 2.17. Cartesian and NMO-coordinate gained outputs. The horizontal axis offset in meters. Both plots are obtained by taking the signed square of migration outputs.

$$t = 2\int_0^D \frac{ds}{v(s)\left[1 - r^2v^2(s)\right]^{1/2}} - \int_0^{z'} \frac{ds}{v(s)\left[1 - r^2v^2(s)\right]^{1/2}} \tag{9}$$

$$z = z'$$

To get the wave equation in this new coordinate system, the Jacobian of this transformation and its inverse will be needed. Define the Jacobian, J, through the relationship

$$\begin{bmatrix} \frac{\partial}{\partial z'} \\ \frac{\partial}{\partial r} \\ \frac{\partial}{\partial D} \end{bmatrix} = J \begin{bmatrix} \frac{\partial}{\partial z} \\ \frac{\partial}{\partial g} \\ \frac{\partial}{\partial t} \end{bmatrix}$$

The nine coefficients of J can be found by partial differentiation of equations (9). It will be convenient to introduce a new symbol

$$I(r,y) = \int_0^y \frac{v(s)ds}{\left[1 - r^2v^2(s)\right]^{3/2}}$$

where y will typically be taken to be z' or D. This integral appears in expressions for $\partial g / \partial r$ and $\partial g / \partial z$ so its introduction simplifies expressions for J and J^{-1}. Written in integral free form, J is the three by three matrix

$$J = \begin{bmatrix} 1 & \frac{-rv(z')}{\left[1 - r^2v^2(z')\right]^{1/2}} & \frac{-1}{v(z')\left[1 - r^2v^2(z')\right]^{1/2}} \\ 0 & 2I(r,D) - I(r,z') & r\left[2I(r,D) - I(r,z')\right] \\ 0 & \frac{2rv(D)}{\left[1 - r^2v^2(D)\right]^{1/2}} & \frac{2}{v(D)\left[1 - r^2v^2(D)\right]^{1/2}} \end{bmatrix}$$

The coefficients of J are usually written in the (g,z,t) coordinate system. This time we are more interested in J^{-1}, since that matrix can be used to display the wave equation in (r,z',D)-space. If J, as written, is inverted, then the result will be J^{-1} in the desired coordinate system. Performing the matrix inversion,

$$J^{-1} = \begin{bmatrix} 1 & \dfrac{\left[1-r^2v^2(z')\right]^{-1/2}\left[rv^2(z')-rv^2(D)\right]}{v(z')\left[1-r^2v^2(D)\right]\left[2I(r,D)-I(r,z')\right]} & \dfrac{v(D)\left[1-r^2v^2(z')\right]^{1/2}}{2v(z')\left[1-r^2v^2(D)\right]^{1/2}} \\ 0 & \dfrac{1}{\left[1-r^2v^2(D)\right]\left[2I(r,D)-I(r,z')\right]} & \dfrac{-rv(D)}{2\left[1-r^2v^2(D)\right]^{1/2}} \\ 0 & \dfrac{-rv^2(D)}{\left[1-r^2v^2(D)\right]\left[2I(r,D)-I(r,z')\right]} & \dfrac{v(D)}{2\left[1-r^2v^2(D)\right]^{1/2}} \end{bmatrix}$$

The matrix J^{-1} is needed to rewrite the one-way wave equation in (r,z',D)-space. The expression for the one-way upgoing wave equation in the new coordinate system makes use of equations for $\partial^2/\partial g^2$, $v^{-2}(z)\partial^2/\partial t^2$, and $\partial/\partial z$ in the new system. Dropping terms proportional to $\partial/\partial D$ and to $\partial/\partial r$,

$$\frac{1}{v^2(z')}\frac{\partial^2}{\partial t^2} = \frac{r^2v^4(D)}{v^2(z')\left[1-r^2v^2(D)\right]^2\left[2I(r,D)-I(r,z')\right]^2}\frac{\partial^2}{\partial r^2}$$
$$- \frac{rv^3(D)v^{-2}(z')}{\left[1-r^2v^2(D)\right]^{3/2}\left[2I(r,D)-I(r,z')\right]}\frac{\partial^2}{\partial r\,\partial D} + \frac{v^2(D)v^{-2}(z')}{4\left[1-r^2v^2(D)\right]}\frac{\partial^2}{\partial D^2}$$

$$\frac{\partial^2}{\partial g^2} = \frac{1}{\left[1-r^2v^2(D)\right]\left[2I(r,D)-I(r,z')\right]^2}\frac{\partial^2}{\partial r^2}$$
$$- \frac{rv(D)}{\left[1-r^2v^2(z')\right]^{3/2}\left[2I(r,D)-I(r,z')\right]}\frac{\partial^2}{\partial r\,\partial D} + \frac{r^2v^2(D)}{4\left[1-r^2v^2(D)\right]}\frac{\partial^2}{\partial D^2}$$

$$\frac{\partial}{\partial z} = \frac{\partial}{\partial z'} + \frac{v^{-1}(z')\left[rv^2(z')-rv^2(D)\right]}{\left[1-r^2v^2(z')\right]^{1/2}\left[1-r^2v^2(D)\right]\left[2I(r,D)-I(r,z')\right]}\frac{\partial}{\partial r}$$
$$+ \frac{v(D)\left[1-r^2v^2(z')\right]^{1/2}}{2v(z')\left[1-r^2v^2(D)\right]^{1/2}}\frac{\partial}{\partial D}$$

When the above relationships are plugged into the one-way wave equation there will be ambiguity to resolve. There will be many ways in which to approximate the square root. The criterion that will be used here is to derive a partial differential equation that resembles equation (5) as closely as possible. The one way wave equation for upgoing waves is formally

$$\frac{\partial U}{\partial z'} + \left[\frac{\partial U}{\partial z} - \frac{\partial U}{\partial z'}\right] = \left\{\left[\frac{\partial}{\partial z} - \frac{\partial}{\partial z'}\right]^2 + \left[\frac{1}{v^2(z)}\frac{\partial^2}{\partial t^2} - \frac{\partial^2}{\partial g^2} - \left[\frac{\partial}{\partial z} - \frac{\partial}{\partial z'}\right]^2\right]\right\}^{1/2} U \qquad (10)$$

in terminology that mixes coordinate systems. Combining the last four equations yields a form for the one-way wave equation in NMO coordinates. Moreover, the zero order approximation to the square root is of the form $\partial U / \partial z' = 0$ by design. This is the same zero order equation as that found in the constant velocity discussion. Thus, the one-way wave equation is

$$\frac{\partial U}{\partial z'} + \frac{\left[1-r^2v^2(z')\right]^{-1/2}\left[rv^2(z')-rv^{-2}(D)\right]}{v(z')\left[1-r^2v^2(D)\right]\left[2I(r,D)-I(r,z')\right]}\frac{\partial U}{\partial r} + \frac{v(D)\left[1-r^2v^2(z')\right]^{1/2}}{2v(z')\left[1-r^2v^2(D)\right]^{1/2}}\frac{\partial U}{\partial D} =$$

$$\left\{\left[\frac{\left[1-r^2v^2(z')\right]^{-1/2}\left[rv^2(z')-rv^{-2}(D)\right]}{v(z')\left[1-r^2v^2(D)\right]\left[2I(r,D)-I(r,z')\right]}\frac{\partial}{\partial r} + \frac{v(D)\left[1-r^2v^2(z')\right]^{1/2}}{2v(z')\left[1-r^2v^2(D)\right]^{1/2}}\frac{\partial}{\partial D}\right]^2 - \frac{1}{\left[1-r^2v^2(D)\right]\left[1-r^2v^2(z')\right]\left[2I(r,D)-I(r,z')\right]^2}\frac{\partial^2}{\partial r^2}\right\}^{1/2} U$$

Fortunately, this lengthy partial differential equation has a simple fifteen degree approximation. The reason for this is that the leading zero order terms cancel by construction. The result is a partial differential equation like that in equation (5),

$$\frac{2\left[1-r^2v^2(z')\right]^{-1/2}\left[rv^2(z')-rv^2(D)\right]}{v(z')\left[1-r^2v^2(D)\right]\left[2I(r,D)-I(r,z')\right]}\frac{\partial^2 U}{\partial z'\partial r} + \frac{v(D)\left[1-r^2v^2(z')\right]^{1/2}}{v(z')\left[1-r^2v^2(D)\right]^{1/2}}\frac{\partial^2}{\partial z'\partial D} =$$

$$\frac{-1}{\left[1-r^2v^2(D)\right]\left[1-r^2v^2(z')\right]\left[2I(r,D)-I(r,z')\right]^2}\frac{\partial^2 U}{\partial r^2} \qquad (11)$$

with an extra $\partial^2 / \partial z' \partial r$ term.

Lateral varying velocity functions can be incorporated with a thin lens term. Let $\bar{v}(r,z')$ denote the laterally varying acoustic velocity function of the earth and retain $v(z')$ as the transformation velocity for the radial/NMO coordinate

system. Under these circumstances, another term should be included as an argument to the square root function in equation (10). In notation that mixes coordinate systems, the third additive term should be

$$\left[\frac{1}{\bar{v}^2(r,z')} - \frac{1}{v^2(z')}\right]\frac{\partial^2}{\partial t^2}$$

If the 15 degree approximation is applied to the one-way wave equation under these circumstances, the result is a first order equation in z' with two additive terms. This differential equation can be split into two differential equations to be solved in alternating order at every z' step. One of the equations of the split is equation (11), and the other is a thin lens equation

$$\frac{2\left[1-r^2v^2(z')\right]^{-1/2}\left[rv^2(z')-rv^2(D)\right]}{v(z')\left[1-r^2v^2(D)\right]\left[2I(r,D)-I(r,z')\right]}\frac{\partial^2 U}{\partial z'\partial r} + \frac{v(D)\left[1-r^2v^2(z')\right]^{1/2}}{v(z')\left[1-r^2v^2(D)\right]^{1/2}}\frac{\partial^2}{\partial z'\partial D} =$$

$$\left[\frac{v^2(z')}{\bar{v}^2(r,z')} - 1\right]\left\{\frac{r^2v^4(D)}{v^2(z')\left[1-r^2v^2(D)\right]^2\left[2I(r,D)-I(r,z')\right]^2}\frac{\partial^2 U}{\partial r^2}\right.$$

$$\left. - \frac{rv^3(D)v^{-2}(z')}{\left[1-r^2v^2(D)\right]^{3/2}\left[2I(r,D)-I(r,z')\right]}\frac{\partial^2 U}{\partial r\,\partial D} + \frac{v^2(D)v^{-2}(z')}{4\left[1-r^2v^2(D)\right]}\frac{\partial^2 U}{\partial D^2}\right\}$$